The Astrophysical Journal, 647:1535–1542, 2006 August 20

ABSORPTION CROSS SECTIONS OF NH_3, NH_2D, NHD_2, AND ND_3 IN THE SPECTRAL RANGE 140–220 nm AND IMPLICATIONS FOR PLANETARY ISOTOPIC FRACTIONATION

Bing-Ming Cheng,[1] Hsiao-Chi Lu,[1] Hong-Kai Chen,[1] Mohammed Bahou,[2] Yuan-Pern Lee,[2] Alexander M. Mebel,[3] L. C. Lee,[4] Mao-Chang Liang,[5] and Yuk L. Yung[5]

Received 2006 February 9; accepted 2006 May 2

ABSTRACT

Cross sections for photoabsorption of NH_3, NH_2D, NHD_2, and ND_3 in the spectral region 140–220 nm were determined at ~298 K using synchrotron radiation. Absorption spectra of NH_2D and NHD_2 were deduced from spectra of mixtures of NH_3 and ND_3, of which the equilibrium concentrations for all four isotopologues obey statistical distributions. Cross sections of NH_2D, NHD_2, and ND_3 are new. Oscillator strengths, an integration of absorption cross sections over the spectral lines, for both $A \leftarrow X$ and $B \leftarrow X$ systems of NH_3 agree satisfactorily with previous reports; values for NH_2D, NHD_2, and ND_3 agree with quantum chemical predictions. The photolysis of NH_3 provides a major source of reactive hydrogen in the lower stratosphere and upper troposphere of giant planets such as Jupiter. Incorporating the measured photoabsorption cross sections of NH_3 and NH_2D into the Caltech/JPL photochemical diffusive model for the atmosphere of Jupiter, we find that the photolysis efficiency of NH_2D is lower than that of NH_3 by as much as 30%. The D/H ratio in NH_2D/NH_3 for tracing the microphysics in the troposphere of Jupiter is also discussed.

Subject headings: astrochemistry — methods: laboratory — molecular data

1. INTRODUCTION

Ammonia, NH_3, has been observed in the atmospheres of Earth, Jupiter, and Saturn (Dick & Ziko 1973; Yung & DeMore 1999). The cross sections for photoabsorption of NH_3 in the region 140–220 nm have been measured by several groups (Okabe 1978; Suto & Lee 1983; Chen et al. 1999), but those of NH_2D, NHD_2, and ND_3 are unreported. These measurements are important for modeling effects of photoinduced fractionation in various deuterated isotopologues of NH_3 in planetary atmospheres (Cheng et al. 1999; Miller & Yung 2000; Lee et al. 2001).

The $A \leftarrow X$ transition of NH_3 exhibits a discrete progression of features built upon an intense continuum (Okabe 1978; Suto & Lee 1983; Chen et al. 1999; Burton et al. 1993). Line widths for bands associated with levels $v_2' \geq 2$ are large (Douglas 1963; Ziegler 1985; Nakajima et al. 1991) because the A state is essentially repulsive above these levels due to nonadiabatic interactions with the X state (Rosmus et al. 1987; McCarthy et al. 1987; Biesner et al. 1989; Li & Vidal 1994). The lifetime for the $v_2' = 2$ level of NH_3 in the A state is in a range of 70–140 fs (Ziegler 1987; Chung & Ziegler 1988), and lifetimes of higher levels are even smaller. In contrast, bands of the $B \leftarrow X$ transition at low energy exhibit distinct rotational structures (Li & Vidal 1994; Ashfold et al. 1987, 1988); the lifetimes of the B ($v_2' = 0$–6) state are ~6.1 ps for NH_3 and ~250 ps for ND_3, independent of the rotational level (Ashfold et al. 1988).

The oscillator strength for the $A \leftarrow X$ transition (165–220 nm) of NH_3 is calculated to be 0.088 (Runau et al. 1977; Chantranupong et al. 1991), in agreement with experimental measurements (Burton et al. 1993; Watanabe 1954). In contrast, the predicted oscillator strength of 0.002 for the $B \leftarrow X$ transition in the region 143–170 nm (Runau et al. 1977; Chantranupong et al. 1991) is about one-tenth the experimental value (Burton et al. 1993). To resolve this discrepancy, further theoretical and experimental investigations are required. A complete set of measurements for all four deuterated NH_3 isotopologues will, moreover, provide valuable information for verifying the accuracy of theoretical potential energy surfaces (PESs) of these electronically excited states and to assess the effects of isotopic fractionation in planetary atmospheres.

We have carefully determined absorption cross sections in the spectral region 140–220 nm for NH_3 and its deuterated variants. High-level calculations on the A and B states of these species were also performed to assist our understanding of experimental results. The photoinduced isotopic fractionation of NH_2D in the atmosphere of Jupiter is discussed.

2. EXPERIMENT

The experimental setup has been described previously (Cheng et al. 1999, 2002). In brief, vacuum ultraviolet (VUV) light produced in the National Synchrotron Radiation Research Center in Taiwan was dispersed with a high-flux cylindrical-grating monochromator of focal length 6 m. With a grating of 600 grooves mm^{-1} and a slit width of 0.050 mm, a resolution of 0.02 nm was achieved. The wavelengths were calibrated with absorption lines of Xe (Yoshino & Freeman 1985), CO (Tilford et al. 1965; Simmons et al. 1969), O_2 (Yoshino et al. 1984; Smith et al. 2004), and NO (Lagerqvist & Miescher 1958; Engleman et al. 1970; Murray et al. 1994; Yoshino et al. 1998). The accuracy in measurements of wavelength is limited by the scan step, typically 0.02 nm.

The absorption cross sections were measured with a double-beam apparatus. The VUV light was converted to visible light with sodium salicylate coated on a glass window before detection with a photomultiplier tube in a photon-counting mode. The absorption cross section, σ, was determined according to the equation $\ln(I_o/I) = n\sigma L + \alpha$, in which I_o and I are intensities of reflected and transmitted light, respectively, n is the gas density, and $L = 8.9$ cm is the length of the gas cell. The constant α was

[1] National Synchrotron Radiation Research Center, Hsinchu Science Park, Hsinchu 30076, Taiwan.
[2] Department of Applied Chemistry and Institute of Molecular Science, National Chiao Tung University, Hsinchu 30010, Taiwan.
[3] Department of Chemistry and Biochemistry, Florida International University, Miami, FL 33199.
[4] Department of Electrical and Computer Engineering, San Diego State University, San Diego, CA 92182.
[5] Division of Geological and Planetary Sciences, California Institute of Technology, 1200 East California Boulevard, Pasadena, CA 91125.

determined at $n = 0$, when the gas cell was evacuated below 10^{-7} torr; the absorbance A is equal to $n\sigma L$. At each wavelength, the σ value was obtained from a linear least-squares fit of 4–11 measurements at varied gas pressures. To avoid saturation effects, the maximum absorbance was limited to 0.4 for the 140–165 nm region and 1.4 for the 165–220 nm region.

A reservoir of volume about 600 cm^3 was connected to the gas cell so as to maintain a constant gas pressure during data acquisition. The gas densities were determined from pressures measured with four pressure meters (MKS Baratron) covering the range 0.003–1000 torr. The temperature was monitored with a thermocouple.

NH_3 (99.99%, Matheson) and ND_3 (99% isotopic purity, Cambridge Isotope Laboratories) were further purified with a freeze-pump-thaw procedure at 77 K followed by vacuum distillation from 206 to 77 K. NH_2D and NHD_2 were obtained from mixtures of NH_3 and ND_3. The compositions of NH_3, NH_2D, NHD_2, and ND_3 are consistent with a statistical distribution, apart from large experimental uncertainties (Reid et al. 2000; Akagi et al. 2004). We measured infrared absorption spectra of NH_3, ND_3, and two mixtures of NH_3 and ND_3 with initial ratios $[NH_3]/[ND_3] = 2/1$ and 5/7 to determine the concentration of each isotopologue in the mixture; the partition of isotopologues obeys a statistical distribution within experimental uncertainties. For these two mixtures, the final distributions are $[NH_3]:[NH_2D]:[NHD_2]:[ND_3] = 0.2963:0.4444:0.2222:0.0370$ and $0.0723:0.3038:0.4253:0.1985$, respectively. At room temperature and under high pressure, a few days are required for the mixture to reach the statistical equilibrium.

3. THEORETICAL CALCULATIONS

The geometries of NH_3 in the electronic ground and excited states were optimized using the complete active-space self-consistent field (CASSCF) method (Werner & Knowles 1985; Knowles & Werner 1985) and 6-311++G(d,p) basis set with the active space including all eight valence electrons distributed on 13 orbitals. The active orbitals are all valence orbitals and Rydberg $3s$, $3p_x$, $3p_y$, $3p_z$, as well as two $3d$ orbitals with lowest energy. Vibrational wavenumbers were computed for isotopologues NH_3, NH_2D, NHD_2, and ND_3 at the CASSCF(8,13)/6-311++G(d,p) level. Vertical and adiabatic excitation energies were refined employing the internally contracted multireference configuration-interaction (MRCI) method (Werner & Knowles 1988; Knowles & Werner 1988) with the (8,13) active space including single and double excitations and Davidson's correction for quadruple excitation with Dunning's correlation-consistent cc-pVTZ basis set, denoted MRCI+Q(8,13)/cc-pVTZ. Zero-point energy (ZPE) corrections were included in adiabatic excitation energies using unscaled vibrational wavenumbers from the CASSCF(8,13)/6-311++G(d,p) calculations. Oscillator strengths were computed using transition dipole moments obtained with CASSCF(8,13)/6-311++G(d,p) and vertical excitation energies were calculated at the MRCI+Q(8,13)/cc-pVTZ level. All calculations were performed with MOLPRO[6] and DALTON[7] program packages.

The geometric parameters, NH = 1.015 Å and ∠HNH = 107.°5, optimized with CASSCF(8,13)/6-311++G(d,p) for the electronic ground state $X\ ^1A_1$ agree with the experimental values of 1.012 Å and 106.°0, respectively. The first excited state of NH_3, $2\ ^1A_1$, has a $n \rightarrow 3s\ (a_1)$ character. The vertical excitation energy and oscillator strength are calculated to be 5.85 eV and 0.0608, respectively. The geometry of this state was optimized with symmetry constrained to C_s with respect to the mirror plane containing one N−H bond. Within C_s symmetry, this state corresponds to $2\ ^1A'$, but upon optimization the geometry converges to a planar D_{3h} symmetric structure with N−H bond length of 1.046 Å. The electronic terms for the A state within point groups D_{3h} and C_{2v} are $1\ ^1A_2''$ and $1\ ^1B_1$, respectively.

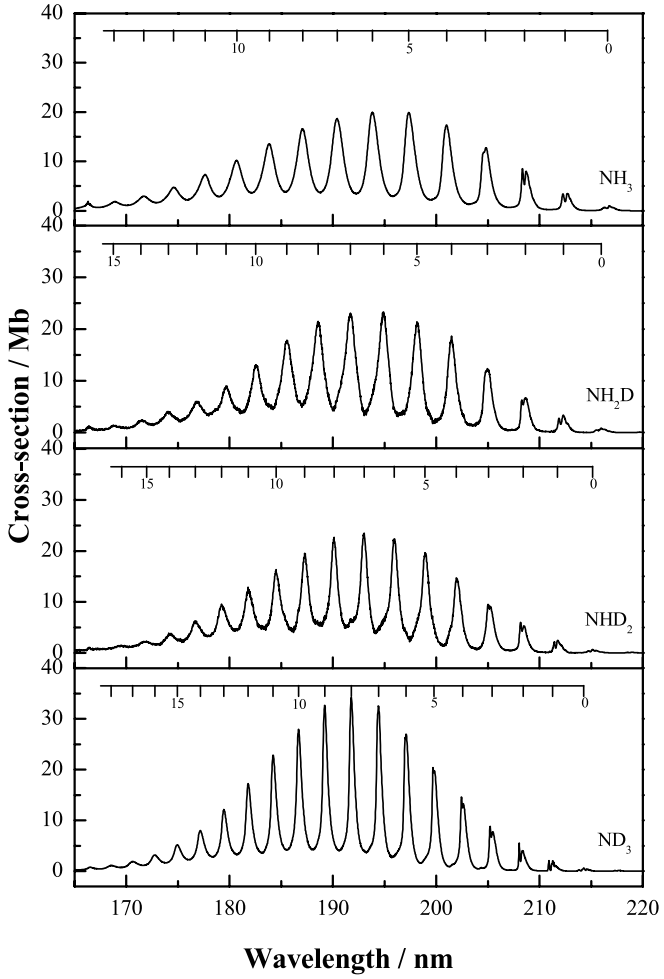

FIG. 1.—Absorption cross sections (in units of Mb, 1 Mb = 10^{-18} cm^2) of NH_3, NH_2D, NHD_2, and ND_3 in the spectral region 165–220 nm.

The second excited state, $1\ ^1E$, exhibits a $n \rightarrow 3p(e)$ character; the calculated vertical excitation energy and oscillator strength are 8.17 eV and 0.0088, respectively. Within C_s symmetry, the $1\ ^1E$ state splits into two components, $1\ ^1A''$ and $3\ ^1A'$. Geometry optimization on the $1\ ^1A''$ surface gives a planar local minimum of C_{2v} symmetry with one shorter ($N-H_{(1)} = 1.021$ Å) and two longer ($N-H_{(2)} = 1.035$ Å) bonds and angles of $\angle H_{(1)}NH_{(2)} = 118.°5$ and $\angle H_{(2)}NH_{(2)} = 123.°0$; this structure is a true local minimum. In contrast, the $3\ ^1A'$ state optimizes to a ($N-H_{(1)} = 1.040$ Å) and two shorter ($N-H_{(2)} = 1.026$ Å) bonds and $\angle H_{(1)}NH_{(2)} = 121.°6$, $\angle H_{(2)}NH_{(2)} = 116.°9$. When symmetry was relaxed, no local minimum was found, and the molecule dissociated upon optimization.

4. RESULTS AND DISCUSSION

4.1. *Absorption Cross Sections*

The absorption cross sections of NH_3, NH_2D, NHD_2, and ND_3 are shown in Figures 1 and 2 for spectral regions 165–220 and

[6] Molecular electronic structure program, release 1.2, written by Helgaker et al. (2001).

[7] Package of ab initio programs written by Werner et al. (2004), University College Cardiff Consultants, Ltd.

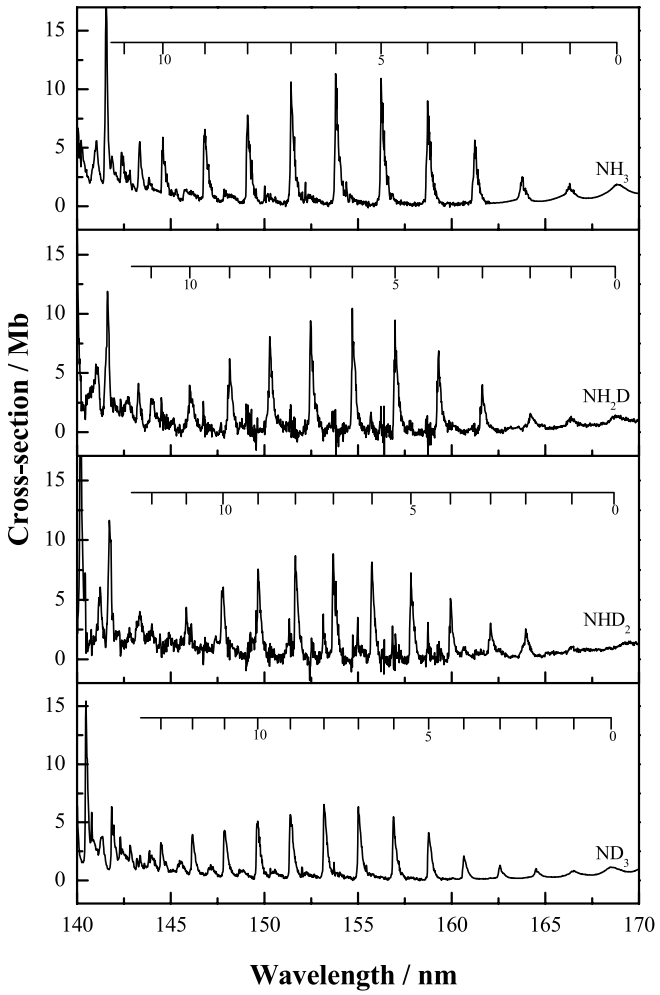

FIG. 2.—Absorption cross sections (in units of Mb, 1 Mb = 10^{-18} cm^2) of NH_3, NH_2D, NHD_2, and ND_3 in the spectral region 140–170 nm.

140–170 nm, respectively. Considering all possible systematic errors, experimental uncertainties of cross sections are estimated to be within 10% of our reported values for NH_3 and ND_3, and 16% for NH_2D and NHD_2. The wavelengths and cross sections at absorption maxima are listed in Tables 1 and 2 for $A \leftarrow X$ and $B \leftarrow X$ transitions, respectively.[8] The band assignments of NH_3 and ND_3 are indicated according to reported high-resolution spectra (Douglas 1963; Walsh & Warsop 1961; Douglas & Hollas 1961). Features of NH_2D and NHD_2 were not assigned previously, but we indicate the vibrational numbering in the figures in accordance with assignments of NH_3 and ND_3. As shown in Figure 1, the bands for the $A \leftarrow X$ transition become narrower and absorption maxima increase as the number of D atoms increases. In contrast, the widths of bands in the $B \leftarrow X$ transition do not alter significantly, but the absorption maxima decrease with the extent of deuteration (as shown in Fig. 2).

The maxima for absorption cross sections of the $A \leftarrow X$ system of NH_3 are in general greater than those of Suto & Lee (1983) by ~10%, but about the same as those of Watanabe (1954). Results for the $B \leftarrow X$ system of NH_3 are about twice those of Suto & Lee (1983) and about 1.3 times those of Watanabe (1954). The deviations in the $B \leftarrow X$ system are due mainly to the varied spectral resolution employed. As in our work we employed a spectral resolution of 0.02 nm, compared to 0.2 nm employed by Suto & Lee (1983); consequently, we obtained greater values for cross sections, especially for the narrow lines in the $B \leftarrow X$ system. A quantitative comparison of oscillator strength avoids this problem (as discussed in § 4.2).

4.2. *Oscillator Strengths*

An integration of absorption cross sections over a spectral range covering all bands of a transition system yields an oscillator strength f that does not depend on experimental bandwidth

[8] Tabulated numerical values of cross sections at intervals of 0.02 nm are available at http://ams-bmc.nsrrc.org.tw.

TABLE 1

PEAK WAVELENGTHS AND CROSS SECTIONS FOR THE $A \leftarrow X$ TRANSITION OF NH_3, NH_2D, NHD_2, AND ND_3

	NH_3		NH_2D		NHD_2		ND_3	
v'	λ (nm)	σ (Mb)	λ (nm)	σ (Mb)	λ (nm)	σ (Mb)	λ (nm)	σ (Mb)
0	216.76	1.00	215.96	0.87	215.14	0.69	214.29	0.67
1	212.72	3.52	212.31	3.44	211.74	2.47	210.92	2.11
2	208.70	8.11	208.71	6.68	208.18	6.02	208.04	5.52
3	204.82	12.80	204.96	12.37	205.02	9.52	205.22	8.82
4	201.02	17.40	201.48	18.67	201.96	14.71	202.44	14.61
5	197.34	19.90	198.14	21.42	198.92	19.65	199.71	20.38
6	193.82	20.00	194.92	23.26	195.94	22.36	197.08	27.02
7	190.42	18.70	191.68	23.12	193.02	23.51	194.41	32.53
8	187.06	16.60	188.58	21.46	190.11	22.63	191.78	34.19
9	183.82	13.60	185.54	17.88	187.28	19.54	189.22	32.66
10	180.66	10.40	182.54	13.08	184.52	16.32	186.68	27.96
11	177.60	7.34	179.64	9.03	181.82	12.89	184.21	22.84
12	174.60	4.55	176.84	6.11	179.21	9.58	181.79	17.24
13	171.68	3.01	174.06	4.11	176.72	6.26	179.44	12.18
14	168.82	1.86	171.42	2.45	174.12	3.88	177.18	8.02
15			168.74	1.45	171.98	2.23	174.94	5.19
16					169.54	1.51	172.76	3.19
17							170.62	1.92
18							168.52	1.14

TABLE 2

PEAK WAVELENGTHS AND CROSS SECTIONS FOR THE $B \leftarrow X$ TRANSITION OF NH_3, NH_2D, NHD_2, AND ND_3

	NH_3		NH_2D		NHD_2		ND_3	
v'	λ (nm)	σ (Mb)	λ (nm)	σ (Mb)	λ (nm)	σ (Mb)	λ (nm)	σ (Mb)
0	168.82	1.89	168.74	1.45	168.66	1.08	168.51	1.14
1	166.31	1.95	166.38	1.33	166.42	1.07	166.52	0.83
2	163.76	2.51	164.19	1.57	163.96	2.54	164.52	1.01
3	161.24	5.64	161.64	4.01	162.08	3.03	162.58	1.29
4	158.72	8.99	159.29	6.86	159.94	5.11	160.64	2.09
5	156.24	10.92	156.98	9.46	157.82	7.24	158.76	4.11
6	153.81	11.31	154.69	10.45	155.74	8.14	156.91	5.47
7	151.42	10.62	152.46	9.42	153.68	8.84	155.02	6.33
8	149.10	7.79	150.28	8.08	151.66	8.68	153.18	6.53
9	146.82	6.56	148.14	6.21	149.66	7.56	151.38	5.67
10	144.58	5.88	146.01	3.97	147.79	6.05	149.64	5.09
11	142.38	4.61	143.96	2.84	145.82	4.35	147.88	4.31
12					143.98	2.98	146.16	3.93
13							144.48	3.22

and might be compared among various experiments. The *f*-value is calculated from (Herzberg 1950)

$$f = 1.13 \times 10^{-6} \int \sigma \, d\overline{\nu}, \qquad (1)$$

where σ is in megabarns, and $\overline{\nu}$ is the wavenumber in cm^{-1}. Values of *f* for both $A \leftarrow X$ (integrated over 165–218 nm) and $B \leftarrow X$ (144–165 nm) systems of all isotopologues are listed in Table 3; those of NH_3 reported by other investigators are also listed for comparison (Burton et al. 1993; Chantranupong et al. 1991; Zeis et al. 1977). Our experimental results of $f = 0.0800$ and 0.0123 for $A \leftarrow X$ and $B \leftarrow X$ transitions of NH_3, respectively, agree satisfactorily with those measured with fast electron impact by Burton et al. (1993) and those from dipole oscillator–strength distributions (Burton et al. 1993; Zeiss et al. 1977). The *f*-value calculated by Chantranupong et al. (1991) agrees with experimental data of the $A \leftarrow X$ transition but is only one-tenth that measured for the $B \leftarrow X$ transition. The *f*-values calculated quantum chemically in this work, 0.0608 and 0.0088 for $A \leftarrow X$ and $B \leftarrow X$ transitions, deviate from our experimental data by 24% and −28%, respectively. The much improved agreement between calculated and experimental oscillator strength for the $B \leftarrow X$ transition results from a much higher level of theory (MRCI, relative to CASSCF employed previously) and a larger active space and superior basis set employed in this work.

To compare with previous measurements, the *f*-value of NH_3 is also determined in the range 170–206 nm; our value of 0.074 is slightly greater than a value of 0.066 reported by Suto & Lee (1983) but smaller than a value of 0.088 reported by Watanabe (1954). The deviations are within experimental uncertainties. The discrepancies might be due to errors in pressure measurements

TABLE 3

COMPARISON OF EXPERIMENTAL AND CALCULATED ADIABATIC EXCITATION ENERGIES AND OSCILLATOR STRENGTHS FOR $A \leftarrow X$ AND $B \leftarrow X$ TRANSITIONS OF NH_3, NH_2D, NHD_2, AND ND_3

Parameter	Method	NH_3	NH_2D	NHD_2	ND_3	Reference
			$A\ ^1A'$			
Energy (cm^{-1})	Expt.	46172	46305	46481	46668	This work
	Calcn.[a]	45952	46064	46183	46305	This work
f (165–218 nm)	Expt.	0.0800	0.0883	0.0811	0.0818	This work
	Expt.[b]	0.0738				Burton et al. 1993
	Expt.[c]	0.0802				Burton et al. 1993; Zeis et al. 1977
	Calcn.	0.0608				This work
	Calcn.	0.0872				Chantranupong et al. 1991
			$B\ ^1A''$			
Energy (cm^{-1})	Expt.	59235	59263	59291	59344	This work
	Calcn.[a]	58986	58989	59073	59164	This work
f (144–165 nm)	Expt.	0.0123	0.0095	0.0112	0.0090	This work
	Expt.[b]	0.0132				Burton et al. 1993
	Expt.[c]	0.0114				Burton et al. 1993; Zeis et al. 1977
	Calcn.	0.0088				This work
	Calcn.	0.0010				Chantranupong et al. 1991

[a] Calculated with MRCI+Q(8,13)/aug-cc-pVTZ//CASSCF(8,13)/6-311++G(d,p) + ZPE[CASSCF(8,13)/6-311++G(d,p)].
[b] Measured from dipole (e,e) spectroscopy.
[c] Measured from dipole oscillator-strength distributions.

of NH_3 that require special attention; NH_3 is adsorbed on the surface easily.

Although absorption maxima and bandwidths of the $A \leftarrow X$ transition varied substantially with the number of D atoms in each isotopologue, the *f*-values of all four isotopologues are almost identical (as indicated in Table 3). Upon considering that the number of D atoms greatly affects the vibrational wavenumbers, these nearly constant *f*-values upon deuteration indicate that vibrational excitation does not affect the absorption cross section of the *A* state. This result is justified by the fact that the PES of the *A* state is crossed with a repulsive surface (Douglas 1963; Chung & Ziegler 1988), so vibrational excitation of the upper state might be unimportant. In contrast, the dissociative continuum might play a significant role in the $A \leftarrow X$ absorption spectrum. This result in turn indicates that the observed vibrational-like structure of the $A \leftarrow X$ transition might be produced by nonadibatic interactions between *A* and *X* states. The "vibrational-like" structures in absorption spectra of the $B \leftarrow X$ transition of H_2O, HDO, and D_2O observed in our laboratory have been fitted satisfactorily with theoretical spectra obtained from quantum dynamical calculations (Van Harrevelt & van Hemert 2000; Cheng et al. 2004). Detailed quantum dynamical calculation on such interaction for NH_3 is desired.

In contrast, the *f*-value of the $B \leftarrow X$ system varies greatly among four isotopologues of NH_3. For instance, the *f*-values of NH_2D and ND_3 are smaller than that of NH_3 by 23%–27%. These results indicate that the $B \leftarrow X$ transition is affected by vibrational excitation. This effect is due to vibronic coupling, which can affect the overall transition dipole moment through the intensity borrowing mechanism (Lin 1976; Liao et al. 1999); hence, vibrational wave functions also contribute to the *f*-value.

Notably, the absorption maxima for the vibrational bands of NHD_2 are generally smaller than those of NH_2D, but the *f*-value of NHD_2 is greater (as listed in Table 3). This increase might be caused by the presence of additional bands due to symmetry breaking; the *B* state of NHD_2 was calculated to belong to point group C_s, whereas NH_3, NHD_2, and ND_3 possess C_{2v} symmetry.

4.3. *Energy and Predissociation of the A State*

The wavenumbers of the band centers, which might not correspond to absorption maxima, of the $A \leftarrow X$ (0,0) transition are listed in Table 3 for all four isotopologues; this value increases from 46,172 cm^{-1} for NH_3 to 46,668 cm^{-1} for ND_3, with intervals of 133, 176, and 187 cm^{-1} for each increase in the number of D atoms. This increase reflects the difference in zero-point energy of the *A* and *X* states when NH_3 becomes progressively deuterated. As seen in Table 3, quantum chemical calculations correctly reproduce this trend. The ZPE-corrected band origins increase from 45,952 cm^{-1} for NH_3 to 46,305 cm^{-1} for ND_3, with intervals of 112, 119, and 122 cm^{-1} as the number of D atoms increases. The agreement between calculated adiabatic excitation energies and experimental values is satisfactory; the differences are smaller than 363 cm^{-1} (0.045 eV).

Although band positions vary, spacings between two neighboring bands are generally consistent with earlier assignments (Douglas 1963; Vaida et al. 1987). Our vibrational spacings, 889, 796, 746, and 663 cm^{-1}, between levels $v_2' = 0$ and 1 of NH_3, NH_2D, NHD_2, and ND_3 are consistent with vibrational wavenumbers of 890, 810, 735, 660 cm^{-1} given by Nakajima et al. (1991) and 892, 813, 738, and 653 cm^{-1} derived by Henck et al. (1995), respectively.

According to our calculations, the normal mode expected to be most active in vibronic spectra corresponding to the $A \leftarrow X$ transition is the umbrella (or inversion, ν_2) mode, which exhibits the largest displacement from the ground to the excited electronic state. The symmetric N—H stretching (ν_1) mode might also contribute to the vibronic structure of the system, but its displacement is much smaller than that for the umbrella mode. The calculated harmonic wavenumbers for ν_2 are 707, 657, 602, and 543 cm^{-1} for the *A* states of NH_3, NH_2D, NHD_2, and ND_3, respectively. These calculated harmonic wavenumbers are significantly smaller than observed vibrational spacings, indicating the highly anharmonic nature of the PES.

The predissociative character of the *A* state was clearly demonstrated by earlier MCSCF calculations of the PES for this state by McCarthy et al. (1987). They showed that NH_3 in this electronic state can dissociate to $NH_2(^2B_1) + H$ overcoming a small barrier of 3226 cm^{-1} at a planar C_{2v} symmetric geometry with $\angle HNH = 113^\circ$, $R_{NH} = 1.042$ Å (in the NH_2 fragment), and $R_{NH} = 1.323$ Å (in the dissociation coordinate). As the dissociative N—H bond elongates further, there arises a conical intersection between the *X* and *A* states. Our present MRCI calculations confirm these conclusions. The scan of the two PESs, performed within C_{2v} symmetry constraints and initiated at the local minimum of the *A* state with all other geometric parameters frozen except increasing one N—H distance, indicate a barrier 2324 cm^{-1} above the local minimum at $R_{NH} \cong 1.3$ Å and crossing of the ground and excited surfaces at $R_{NH} \cong 2.0$ Å. Within C_{2v} symmetry, the *A* state of NH_3 is $^1B_1$ and correlates directly with the ground-state products $NH_2(^2B_1) + H(^2S)$. In contrast, the *X* state is $^1A_1$ and correlates with products in the excited state, $NH_2(^2A_1) + H(^2S)$.

4.4. *Band Origin and Progressions of the B ← X System*

The wavenumbers for band centers of the $B \leftarrow X$ system of NH_3 agree with literature values within 0.05 nm (Li & Vidal 1994; Ashfold 1987, 1988; Langford 1998). Our data for ND_3 also agree with previous reports (Chung & Ziegler 1988; Li & Vidal 1995), except the $v' = 0$ band, for which our wavenumber of 59,344 cm^{-1} is 47 cm^{-1} smaller than the value given by Ashfold et al. (1987, 1988). This discrepancy is too large to be ascribed to experimental uncertainties. On examining the spectra of all four isotopologues shown in Figure 2, we believe that our values are reasonable.

The wavenumber of the origin band increases from 59,235 cm^{-1} for NH_3 to 59,344 cm^{-1} for ND_3. This small increase indicates that changes in zero-point energies of both *B* and *X* states upon deuterization are similar. Calculated band origins for the $B \leftarrow X$ transitions increase from 58,986 cm^{-1} for NH_3 to 59,164 cm^{-1} for ND_3, in agreement with experimental results. For this transition, the difference between the theoretical and experimental adiabatic excitation energies is smaller than 274 cm^{-1} (0.034 eV).

The spectral data for the $B \leftarrow X$ transition of NH_2D and NHD_2 are much less studied than those of NH_3 and ND_3. The first spacings for the $B \leftarrow X$ transition of NH_2D and NHD_2 are 841 and 798 cm^{-1}, intermediate between values of 894 and 709 cm^{-1} for NH_3 and ND_3, respectively. According to our calculations, similar to the $A \leftarrow X$ transition, the most active mode in the $B \leftarrow X$ system is the umbrella (or inversion) mode; calculated harmonic wavenumbers are 870, 811, 743, and 668 cm^{-1} for the *B* state of NH_3, NH_2D, NHD_2, and ND_3, respectively. These calculated harmonic wavenumbers are 2.7%–6.9% smaller than observed spacings between two bands with the smallest wavenumbers.

As shown in Figure 2, some weak bands in spectra of NH_2D and NHD_2 might be due to uncertainties propagated from data manipulation to derive their cross sections from those determined with isotopic mixtures, but the additional progressions for NHD_2 are real and might become active when the C_{2v} symmetry of the *B* state is relaxed to C_s, according to our calculations. Observed

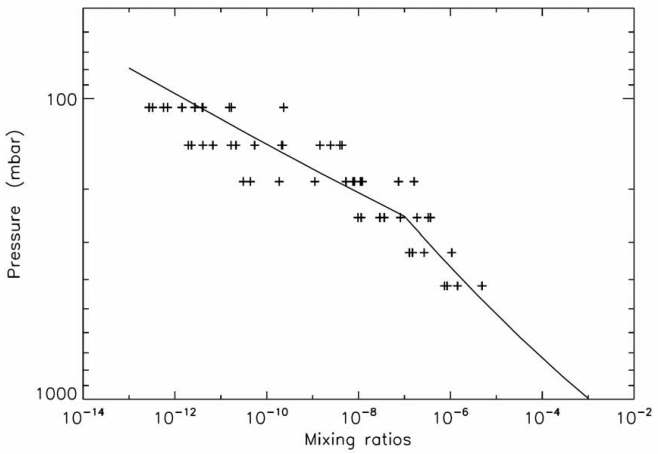

FIG. 3.—Vertical profile of NH_3 (*solid line*) used in the model. Plus signs are measurements by Edgington et al. (1999). Mixing ratio of NH_3 is defined as the number density of NH_3 divided by the number density of the atmosphere in Jupiter.

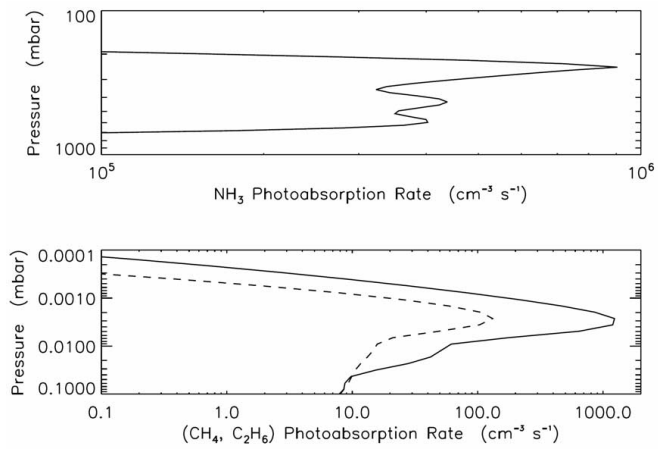

FIG. 4.—Vertical profiles of photoabsorption rates for (*top*) NH_3, (*bottom*; *solid line*) CH_4, and (*bottom*; *dashed line*) C_2H_6.

first spacing of $\sim$753 cm^{-1} for this additional progression of NHD_2 is smaller than the corresponding spacing of $\sim$798 cm^{-1} for the umbrella mode, consistent with an expectation of an assignment of this additional progression to a combination band involving the umbrella motion and other vibrational modes yet to be identified.

4.5. *Implications for the Atmosphere of Jupiter*

The deuterium to hydrogen (D/H) ratio provides an important constraint to the chemical and physical processes in the atmospheres of planets (Owen & Encrenaz 2003). For example, the D/H ratio of water (HDO vs. H_2O) in the upper atmosphere of Mars can be satisfactorily explained by photolytic (Cheng et al. 1999; Miller & Yung 2000) and condensation/evaporation processes (Bertaux & Montmessin 2001). The D/H ratios for HD/H_2 (Encrenaz et al. 1996; Mahaffy et al. 1998; Lellouch et al. 2001) and CH_3D/CH_4 (Encrenaz et al. 1999; Lellouch et al. 2001) in the atmosphere of Jupiter are $\sim 2.3 \times 10^{-5}$. The isotopic composition other than these two species in Jupiter has not been obtained. A theoretical study conducted by Lee et al. (2001) shows that C_2H_6, which is the most abundant hydrocarbon compound produced photochemically via the photolysis of CH_4 in the upper atmosphere of Jupiter, is enriched in D. The predicted D/H ratio in C_2H_5D/C_2H_6 is about 15 times that of HD/H_2 or CH_3D/CH_4. In the lower atmosphere, the photolytically initiated isotopic fractionation processes for hydrocarbon chemistry that operate in the upper atmosphere are severely curtailed by the shielding at wavelengths $<$160 nm due to CH_4 and C_2H_6. The photolytic processes of NH_3, driven by photons with wavelengths $<$230 nm, in the lower stratosphere and upper troposphere are the most significant disequilibrium processes (Strobel 1975). To evaluate the process on the D/H ratios for NH_3 photolytic products, we perform a one-dimensional kinetics simulation incorporating the newly measured photoabsorption cross sections of NH_3 and NH_2D for this region of the atmosphere of Jupiter.

The one-dimensional Caltech/JPL KINETICS model is used in our study. A detailed description of the model has been given previously (e.g., Gladstone et al. 1996). Figure 3 shows the vertical profile of NH_3 adopted in this study (*solid line*). It is based on data from Edgington et al. (1999) (*plus signs* in Fig. 3). Figure 4 shows the vertical profiles of the photoabsorption rates of NH_3. For comparison, we also include results for CH_4 and C_2H_6 from Gladstone et al. (1996) and Lee et al. (2001). As stated earlier, the photoabsorption of CH_4 is significant in the region above $\sim$0.1 mbar pressure level, and NH_3 molecules become the dominant UV absorbers below $\sim$200 mbar. The photolytic products of NH_3 such as H, NH, and NH_2 could react with C_2H_6 in the lower stratosphere/upper troposphere and thereby modify the D/H ratio in ethane that is initially produced in the upper atmosphere of Jupiter. The fractionation of photoabsorption coefficients (*J*-value) for ammonia is presented in Figure 5. It is shown that the photolysis of ammonia will cause the photolytic products of ammonia to be isotopically depleted compared with their parent molecules, ammonia. Therefore, the predicted enhanced D/H ratio in ethane mediated by CH_4 photolysis alone (Lee et al. 2001) may be affected. A simple order-of-magnitude argument is used to estimate the influence of the ammonia photolysis. It is known that the isotopic exchange reaction between D and H_2 is fast (e.g., Lee et al. 2001). The exchange timescale is on the order of 10^3 s at 300 mbar, while the ammonia photolysis is as large as 10^7 s. So the ammonia photolytic effect on other species is severely

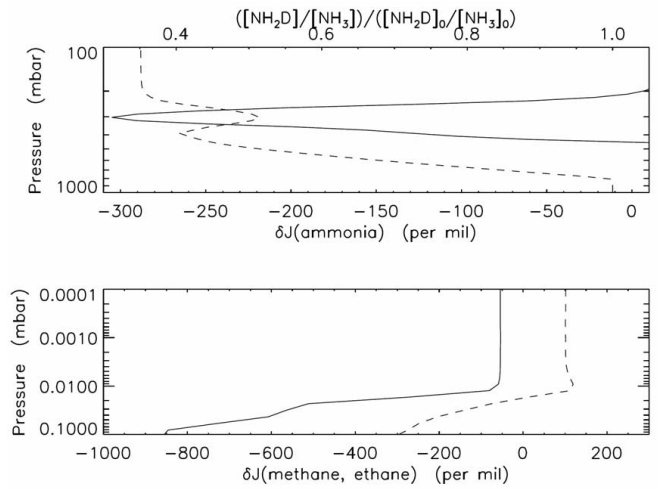

FIG. 5.—Fractionation in *J*-value for (*top*) ammonia, (*bottom*; *solid line*) methane, and (*bottom*; *dashed line*) ethane. The *J*-value is calculated as the product of the absorption cross section of the molecule being photolyzed and the solar flux, all integrated over the wavelength region of interest; δJ(per mil) = $1000 \times [J(\text{deuterated})/J(\text{normal}) - 1]$. The dashed line in the top panel represents the abundance ratio of [NH_2D] and [NH_3], referenced to the value ([NH_2D]$_0$ and [NH_3]$_0$) in the deep atmosphere; both photolysis- and condensation-induced isotopic fractionation are included. See text for details.

diluted. To our knowledge, there is no significant chemical source of ammonia in the troposphere of Jupiter, and the isotopic exchange between ammonia and molecular hydrogen is slow. So the ammonia isotopic fractionation arises mainly from photolysis and condensation/evaporation processes. We will discuss this in a future paper.

In this work, we find that the maximum isotopic fractionation of ammonia due to photolysis is ~ -300 per mil (-300 parts in thousand) at $\sim$300 mbar. However, it is generally believed that ammonia could condense to form clouds in the troposphere (West et al. 1986). The condensation and evaporation of ammonia would be analogous to that of water, which produces water vapor to be isotopically depleted in the upper atmosphere of Mars compared with that in the lower atmosphere (Bertaux & Montmessin 2001). We follow Bertaux & Montmessin's (2001) method to calculate the isotopic fractionation due to condensation but take the precipitation of ammonia into account, because the precipitation in the regions of interest ($\sim$300 mbar) is more important than the photolysis. The precipitation rate is estimated based on the ammonia mixing ratio profile shown in Figure 3. By mass conservation, the precipitation rate is equal to the difference between the diffusion (based on Fig. 3) and photolysis rates (Fig. 4). Assuming the ammonia abundance in the deep atmosphere to be 2×10^{-3}, we find that ammonia can condense in the regions between $\sim$400 and 800 mbar. Above the 400 mbar level the ammonia photochemistry dominates. Below the 800 mbar level the temperature is too warm to allow the precipitation. Since the fractionation factor α for the condensation of NH_2D has not been measured but the value has been determined for ND_3 (Kirshenbaum & Urey 1942; Jancso & van Hook 1974), we follow the typical assumption that $\alpha(NH_2D) = \alpha^{1/3}(ND_3)$. The result after including the photolytic processes is shown by the dashed line in the top panel of Figure 5. We see that the NH_2D abundance is depleted by a factor of $\sim$2 at 300 mbar. So the isotopic composition of ammonia provides a sensitive tool for understanding the microphysics and meteorology in the troposphere of Jupiter.

Our work provides the magnitude of the isotopic effect of ammonia due to photolysis and condensation. Future observations and modeling of the D/H ratios in ammonia are needed to advance our understanding of the chemistry and the microphysics (and dynamics) involving ammonia in the troposphere of Jupiter. Note that the fractionation factor α used in the above calculation is extrapolated from the values measured at higher temperature ($\sim$200 vs. 130 K for the regions of interest in Jupiter). Laboratory measurements of vapor pressures of various ammonia isotopologues at $\sim$130 K are needed to verify or quantify the above calculations.

5. CONCLUDING REMARKS

We determined absorption cross sections and oscillator strengths of NH_3 in four deuterated isotopologues over the spectral range 140–220 nm. Measurements of cross sections of NH_2D, NHD_2, and ND_3 are new. The oscillator strengths for the $A \leftarrow X$ transition of NH_3, NH_2D, NHD_2, and ND_3 in the range 165–218 nm are evaluated to be 0.0800, 0.0883, 0.0811, and 0.0818, respectively; the value for NH_3 agrees with previous experimental and theoretical reports. The oscillator strengths for the $B \leftarrow X$ transition in the range 144–165 nm were determined to be 0.0123, 0.0095, 0.0112, and 0.0090 for NH_3, NH_2D, NHD_2, and ND_3, respectively; the experimental value for NH_3 is slightly greater than our theoretical calculations, but about tenfold of previous predictions. Coupled with those of NH_3, they provide a complete set of data for planetary modeling and further theoretical investigations. Unlike that of the $A \leftarrow X$ transition, the oscillator strength of the $B \leftarrow X$ transition varies with progressive deuteration of NH_3. Additional progressions appear in the $B \leftarrow X$ system of NHD_2 due to symmetry breaking.

Quantum chemical predictions for band origins and oscillator strengths of both transitions agree satisfactorily with experimental results. The umbrella mode is predicted to be active in both transitions. The A state is highly predissociative. The present calculations also predict oscillator strengths for the $B \leftarrow X$ transition of NH_3 much nearer the experimental value than those predicted previously. Incorporating the measured photoabsorption cross sections of NH_3 and NH_2D to the Caltech/JPL KINETICS model for the atmosphere of Jupiter, we find that NH_2D is enriched when compared with NH_3. After taking the isotopic fractionation due to condensation into account, the abundance of NH_2D at $\sim$300 mbar is depleted by a factor of 2. Thus, the isotopic composition of ammonia provides a useful tracer for studying the formation of ammonia cloud in the troposphere of Jupiter.

B.-M. C. and Y.-P. L. thank the National Science Council of Taiwan (grants NSC93-2113-M-213-002 and NSC93-2113-M-009-019) for support. L. C. L. thanks for the National Synchrotron Radiation Research Center in Taiwan for a visiting professorship. M.-C. L. and Y. L. Y. were supported by NASA grant NASA5-13296 to the California Institute of Technology.

REFERENCES

Akagi, H., Yokoyama, K., & Yokoyama, A. 2004, J. Chem. Phys., 120, 4696
Ashfold, M. N. R., Dixon, R. N., Little, N., Stickland, R. J., & Western, C. M. 1988, J. Chem. Phys., 89, 1754
Ashfold, M. N. R., Dixon, R. N., Stickland, R. J., & Western, C. M. 1987, Chem. Phys. Lett., 138, 201
Bertaux, J. L., & Montmessin, F. 2001, J. Geophys. Res. Planets, 106, 32879
Biesner, J., Schnieder, L., Ahlers, G., Xie, X., Welge, K. H., Ashfold, M. N. R., & Dixon, R. N. 1989, J. Chem. Phys., 91, 2901
Burton, G. R., Chan, W. F., Cooper, G., Brion, C. E., Kumar, A., & Meath, W. J. 1993, Can. J. Chem., 71, 341
Chantranupong, L., Hirsch, G., Buenker, R. J., Kimura, M., & Dillon, M. A. 1991, Chem. Phys., 154, 13
Chen, F. Z., Judge, D. L., Wu, C. Y. R., & Caldwell, J. 1999, Planet. Space Sci., 47, 261
Cheng, B.-M., Chew, E. P., Liu, C.-P., Bahou, M., Lee, Y.-P., Yung, Y. L., & Gerstell, M. F. 1999, Geophys. Res. Lett., 26, 3657
Cheng, B.-M., Chung, C.-Y., Bahou, M., Lee, Y.-P., & Lee, L. C. 2002, J. Chem. Phys., 117, 4293
Cheng, B.-M., Chung, C.-Y., Bahou, M., Lee, Y.-P., Lee, L. C., van Harrevelt, R., & van Hemert, M. C. 2004, J. Chem. Phys., 120, 224
Chung, Y. C., & Ziegler, L. D. 1988, J. Chem. Phys., 89, 4692
Dick, K. A., & Ziko, A. O. 1973, ApJ, 182, 609
Douglas, A. E. 1963, Discuss. Faraday Soc., 35, 158
Douglas, A. E., & Hollas, J. M. 1961, Can. J. Phys., 39, 479
Edgington, S. G., Atreya, S. K., Trafton, L. M., Caldwell, J. J., Beebe, R. F., Simon, A. A., & West, R. A. 1999, Icarus, 142, 342
Encrenaz, T., Drossart, P., Feuchtgruber, H., Lellouch, E., Bezard, B., Fouchet, T., & Atreya, S. K. 1999, Planet. Space Sci., 47, 1225
Encrenaz, T., et al. 1996, A&A, 315, L397
Engleman, R., Jr., Rouse, P. E., Peek, H. M., & Baiamonte, V. D. 1970, Beta and Gamma Band Systems of Nitric Oxide, Report LA-4363 (Los Alamos: LASL)
Gladstone, G. R., Allen, M., & Yung, Y. L. 1996, Icarus, 119, 1
Henck, S. A., Mason, M. A., Yan, W.-B., Lehmann, K. K., & Coy, S. L. 1995, J. Chem. Phys., 102, 4772
Herzberg, G. 1950, Molecular Spectra and Molecular Structure I (New York: Van Nostrand)
Jancso, G., & van Hook, W. A. 1974, Chem. Rev., 74, 689
Kirshenbaum, I., & Urey, H. C. 1942. J. Chem. Phys., 10, 706
Knowles, P. J., & Werner, H.-J. 1985, Chem. Phys. Lett., 115, 259
———. 1988, Chem. Phys. Lett., 145, 514
Lagerqvist, A., & Miescher, E. 1958 Helv. Phys. Acta, 31, 221

Langford, S. R. , Orr-Ewing, A. J., Morgan, R. A., Western, C. M., Rijkenberg, A., Scheper, C. R., Buma, W. J., & de Lange, C. A. 1998, J. Chem. Phys., 108, 6667
Lee, A. Y. T., Yung, Y. L., Cheng, B. M., Bahou, M., Chung, C. Y., & Lee, Y. P. 2001, ApJ, 551, L93
Lellouch, E., Bezard, B., Fouchet, T., Feuchtgruber, H., Encrenaz, T., & de Graauw, T. 2001, A&A, 370, 610
Li, X., & Vidal, C. R. 1994, J. Chem. Phys., 101, 5523
———. 1995, J. Chem. Phys., 102, 9167
Liao, D.-W., Mebel, A. M., Hayashi, M., Shiu, Y. J., Chen, Y.-T., & Lin, S. H. 1999, J. Chem. Phys., 111, 205
Lin, S. H. 1976, Proc. R. Soc. London A, 352, 57
Mahaffy, P. R., Donahue, T. M., Atreya, S. K., Owen, T. C., & Niemann, H. B. 1998, Space Sci. Rev., 84, 251
McCarthy, M. I., Rosmus, P., Werner, H.-J., Botschwina, P., & Vaida, V. 1987, J. Chem. Phys., 86, 6693
Miller, C. E., & Yung, Y. L. 2000, J. Geophys. Res. Atmos., 105, 29039
Murray, J. E., Yoshino, K., Esmond, J. R., Parkinson, W. H., Sun, Y., Dalgarno, A., Thorne, A. P., & Cox, G. 1994, J. Chem. Phys., 101, 62
Nakajima, A., Fuke, K., Tsukamoto, K., Yoshida, Y., & Kaya, K. 1991, J. Phys. Chem., 95, 571
Okabe, H. 1978, Photochemistry of Small Molecules (New York: Wiley)
Owen, T., & Encrenaz, T. 2003, Space Sci. Rev., 106, 121
Reid, J. P., Loomis, R. A., & Leone, S. R. 2000, J. Chem. Phys., 112, 3181
Rosmus, P., Botschwina, P., Werner, H.-J., Vaida, V., Engelking, P. C., & McCarthy, M. I. 1987, J. Chem. Phys., 86, 6677
Runau, R., Peyerimhoff, S. D., & Buenker, R. J. 1977, J. Mol. Spectrosc., 68, 253
Simmons, J. D., Bass, A. M., & Tilford, S. G. 1969, ApJ, 155, 345
Smith, P. L., et al. 2004, CfA Molecular Data (Cambridge: H-S CfA), http://www.cfa.harvard.edu/amdata/ampdata/cfamols.html
Strobel, D. F. 1975, Rev. Geophys. 13, 372.
Suto, M., & Lee, L. C. 1983, J. Chem. Phys., 78, 4515
Tilford, S. G., Vanderslice, J. T., & Wilkinson, P. G. 1965, Can. J. Phys., 43, 450
Vaida, V., McCarthy, M. I., Engelking, P. C., Rosmus, P., Werner, H. J., & Botschwina, P. 1987, J. Chem. Phys., 86, 6669
van Harrevelt, R., & van Hemert, M. C. 2000, J. Chem. Phys., 112, 5787
Walsh, A. D., & Warsop, P. A. 1961, Trans. Faraday Soc., 57, 345
Watanabe, K. 1954, J. Chem. Phys., 22, 1564
Werner, H.-J., & Knowles, P. J. 1985, J. Chem. Phys., 82, 5053
———. 1988, J. Chem. Phys., 89, 5803
West, R. A., Strobel, D. F., & Tomasko, M. G. 1986, Icarus, 65, 161
Yoshino, K., & Freeman, D. E. 1985, J. Opt. Soc. Am. B, 2, 1268
Yoshino, K., Freeman, D. E., & Parkinson, W. H. 1984, J. Phys. Chem. Ref. Data, 13, 207
Yoshino, K., et al. 1998, J. Chem. Phys., 109, 1751
Yung, Y. L., & DeMore, W. B., ed. 1999, Photochemistry of Planetary Atmospheres (New York: Oxford Univ. Press)
Zeiss, G. D., Meath, W. J., MacDonald, J. C. F., & Dawson, D. J. 1977, Can. J. Phys., 55, 2080
Ziegler, L. D. 1985, J. Chem. Phys., 82, 664
———. 1987, J. Chem. Phys., 86, 1703